European Journal of Medicinal Chemistry 70 (2013) 607–612

Contents lists available at ScienceDirect

European Journal of Medicinal Chemistry

journal homepage: http://www.elsevier.com/locate/ejmech

Preliminary communication

Skeletal hybridization and PfRIO-2 kinase modeling for synthesis of α-pyrone analogs as anti-malarial agent

Afsana Parveen [a], Arnish Chakraborty [b], Ananda Kumar Konreddy [a], Harapriya Chakravarty [a], Ashoke Sharon [a], Vishal Trivedi [b,**], Chandralata Bal [a,*]

[a] Department of Applied Chemistry, Birla Institute of Technology, Mesra, Ranchi 835215, India
[b] Malaria Research Group, Department of Biotechnology, Indian Institute of Technology, Guwahati 781039, Assam, India

ARTICLE INFO

Article history:
Received 13 July 2013
Received in revised form
19 September 2013
Accepted 11 October 2013
Available online 23 October 2013

Keywords:
Anti-malarial
Pyrone analogs
Plasmodium falciparum
RIO2 kinase
Molecular modeling
Induced fit docking

ABSTRACT

The pharmacophoric hybridization and computational design approach were applied to generate a novel series of α-pyrone analogs as plausible anti-malarial lead candidate. A putative active site in flexible loop close to wing-helix domain of PfRIO2 kinase was explored computationally to understand the molecular basis of ligand binding. All the synthesized molecules (**3a**–**g**) exhibited *in vitro* antimalarial activity. Oxidative stress induced by **3a**–**d** were calculated and found to be significantly higher in case of **3b**. Therefore, **3b**, which shown most significant result was identified as promising lead for further SAR study to develop potent anti-malarials.

1. Introduction

Malaria is a protozoal parasitic disease that causes millions of death worldwide every year. In addition, the treatment is becoming more and more difficult because of emergence of drug-resistant malaria. Artemisinin combination therapy (ACT) has been useful over past decades [1], but the recent emergence of ACT resistance [2] provides strong motivation to discover new potential antimalarial drugs. Parasite growth and ability to maintains stress is linked to the down-stream signaling and ribosome biogenesis [3]. RIO like kinase, RIO-1 (PFL1490w) and RIO-2 kinase (PFD0975w) are present in the malaria kinome with uncharacterized function (www.plasmodb.org). Structural characterization of PFD0975w, the RIO-2 kinase of Plasmodium Falciparum (PfRIO-2 kinase) indicates N-terminal DNA binding winged helix domain (1–84), a linker region (85–147) and C-terminal kinase domain (148–275). It has a well defined ATP binding pocket and is significantly different than the human RIO-2 kinase [4]. Further, the absence of activation loop and distinguished structural features of PfRIO-2 kinase provides an opportunity to explore it as a new drug target [4]. Recently, naturally occurring bioactive molecules and selected heterocycles were screened against PfRIO-2 kinase, which allow us to delineate pharmacological points required for inhibitor development against PfRIO-2 kinase [5,6].

Febrifugine (**I**, Fig. 1), a natural product with high anti-malarial activity [7]. was isolated in 1947 from the roots of a Chinese shrub, *Chang Shan*. The 4-quinazolinone moiety, 1′-amino and C-2′ as well as C-3″O-functionalities are crucial for the anti-malarial activity of febrifugine [8]. Argentilactone (**II**, Fig. 1), isolated from the roots and the leaves of *Raimondia cf. monoica* was found to have ED_{50} of 0.1 μg/mL against *Plasmodium falciparum* (*P. falciparum*) [9]. It was the first report of α-pyrone derivative having anti-malarial activity. However, due to toxicity [9,10] both these molecules couldn't develop as a clinical drug. Recently, 4(1*H*)-quinolone ester derivatives (**III**, Fig. 1) with two close keto groups have been considered as promising anti-malarials needing further SAR and optimization [11]. In our ongoing anti-malarial lead identification project, we intended to apply hybridization of the identified pharmacophores (Fig. 1) and generated a novel α-pyrone skeleton (**IV**, Fig. 1). In the current work, we carried out detailed *in-silico*

Abbreviations: RIO2 kinase, right open reading frame 2 kinase; PfRIO2 kinase, *Plasmodium falciparum* RIO2 kinase; ATP, adenosine triphosphate; DNA, deoxyribonucleic acid; w-HTH, wing helix domain.

* Corresponding author. Tel.: +91 651 2276531; fax: +91 651 2275401.
** Corresponding author. Tel.: +91 361 2582217; fax: +91 361 258 2249.
E-mail addresses: vtrivedi@iitg.ernet.in, Vishalash_1999@yahoo.com (V. Trivedi), chandralata.bal@gmail.com, cbal@bitmesra.ac.in (C. Bal).

0223-5234/$ – see front matter © 2013 Elsevier Masson SAS. All rights reserved.
http://dx.doi.org/10.1016/j.ejmech.2013.10.028

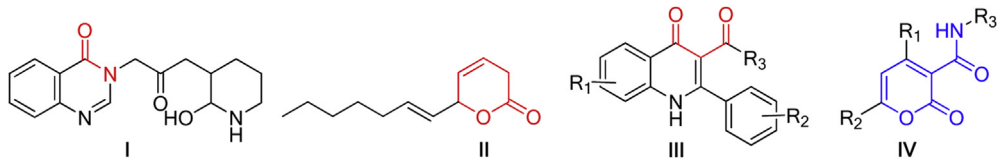

Fig. 1. Structures of reported potent antimalarials (**I**–**III**), identified pharmacophores (red) for hybridization and newly generated hybridized skeleton (blue). (For interpretation of the references to color in this figure legend, the reader is referred to the web version of this article.)

studies (modeling, docking and binding mode analysis) of our newly generated α-pyrone derivatives (**IV**, Fig. 1) to analyze whether they could be potential antimalarials exploiting PfRIO2 kinase. The synthesized molecules were evaluated for their anti-malarial potential. One lead molecule of this novel class was identified for further optimization and mode of action study.

2. Results and discussion

2.1. Molecular modeling

Recently, we developed and explored the 3D structural aspect of PfRIO2 kinase [4,12] as plausible novel anti-malarial drug target to support our anti-malarial drug discovery program. In the present study, the binding sites were identified using SiteMap module of Schrödinger Suite. Four binding sites were identified and named as S1, S2, S3 and S4 (Fig. 2a). The S1 is found within the flexible loop region and close to DNA binding region (wing helix Domain). The S1 site comprised of E104, S105, D106, I107, K121, L125, R127, L163, P174, S187, I189, G191, P193, N227, N230, K232, I242, D243, P245. The S2 subsite is the major groove and known for ATP binding and contains major residues K2, D4, I5, F8, D79, F80, L83, I95, Y108, L120, I122, and M183. The subsite S3 found near to C-terminal was surrounded by S129, F130, R131, I133, N135, Y139, G141, and K142. The amino acid residues L250, R251, H252, V253, A255, K256, P282 formed the S4 subsite. The S3 and S4 are very small and close to surface, which may not be suitable for inhibitor binding. Since the active site is not yet identified, we studied the ligand interactions to S1 and S2 sites of PfRIO2. The protein–ligand interaction study was carried out with two complex models of the protein. The 1st complex comprised both ATP and DNA, while in the 2nd complex only DNA was present. Therefore, in the 2nd complex, ligand can

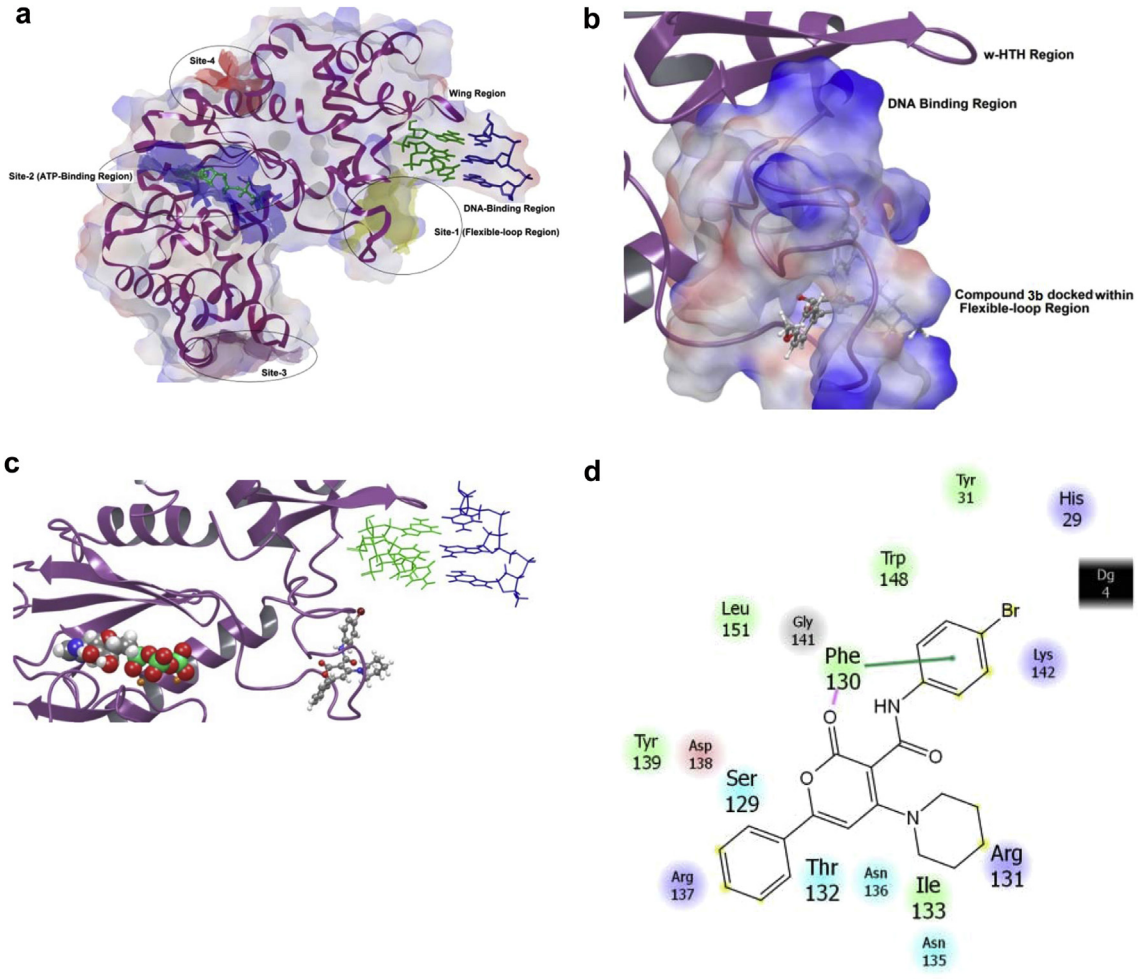

Fig. 2. a) The SiteMap analysis of PfRIO2 kinase showing the four locations as plausible ligand binding site. b) The surface diagram showing the binding of **3b** into S1 site. c) The docked pose of **3b** in the S1 site. d) Ligand–receptor interaction diagram showing the major hot spot residues of flexible loop interacting with **3b**.

utilize the full site including the space of ATP. The ligand structures were built using Maestro interface of and their conformations were optimized by LigPrep. The optimized ligands were docked by default protocols to S1 and S2 sites of the above mentioned two types of PfRIO2 complex using Glide [13]. However the standard docking results didn't show significant interactions and binding energy score. The poor results obtained may be due to the requirement of additional enzyme flexibility within the site. Thus the induced fit docking (IFD) protocols [14] were implemented to conduct the docking experiment followed by side chain refinement using Prime. The prime refinement ensures protein side chain flexibility according to ligand fitting into the active site. This was necessary because the actual conformation of the active site in PfRIO2 is not yet known. When the receptor flexibility was considered, the ligand–protein interactions were found significant in S1 site. It is interesting to note that the molecular docking and interaction profile were found better in the 1st complex model. Therefore, all the docking experiments were conducted on this complex using S1 active site located in the flexible loop region. Fig. 2b is a surface diagram showing binding of **3b** (the most active compound) in the S1 site. Docked pose of **3b** (Fig. 2c) was created to have a more closer look into its binding mode into the flexible loop region near to the DNA binding region. Ligand–receptor interactions were studied in detail and shown in Fig. 2d. This analysis highlighted the major hot spot residues in the flexible loop (hydrophobic: Tyr139, Leu151, Trp148, Tyr31, Ile133, Phe130; acidic: Asp 138; polar/hydrophilic: Ser129, Thr132, Asn136, Asn135; basic: Arg137, Arg131, Lys142, His29) interacting with **3b**. Among them one of the hydrophobic residues Phe130 also forms a $\pi\cdots\pi$ stacking with bromophenyl ring of **3b**. Dg4 (black block in Fig. 2d) indicates the presence of DNA in proximity. The IFD dockings were further scored by extra precision scoring function within the S1 active site to evaluate the energetic preference of compounds and the binding profile results are summarized in Table 1. The negative eMBrAcE (Multi-ligand Bimolecular Association with Energetic) score suggests binding of the ligand with PfRIO2 kinase to lower the energy of PfRIO2–ligand complex. This result also supports the suitability of S1 to be considered as active site. The energetic scores are based on semi-empirical calculation and may not correlate exactly with biological activity, they reveal the possibly of the ligand binding in this novel target enzyme. Ligand binding affinity was also estimated by Glide Emodel score (Table 1). Emodel score is the combination of GlideScore (GScore) and nonbonded interaction energy. The four molecules **3a**–**3d** shown favorable energy score and interestingly the same were found significant in biological screening. In absence of any ligand or inhibitor reported for PfRIO2 kinase, chloroquine, a potent antimalarial was selected for possible comparison. The poor binding score (Table 1) of chloroquine with PfRIO2 limits the possibility of chloroquine–PfRIO2 binding. The significant binding score of some of the synthesized compounds suggest the plausible anti-malarial activity through PfRIO2 kinase inhibition. However more specific biological screening is necessary in future to confirm the mode of action of these class of compounds (Scheme 1).

Table 1
In-silico binding analysis by Glide and eMBrAcE score.

S. No	Compound	Docking[a]	eMBrAcE score[b] (energy difference)		
		Glide Emodel score	*VdW*	Electrostatic	Total (ΔE)
1	**3a**	−72.8	−181.8	−139.0	−140.7
2	**3b**	−78.9	−178.3	−185.3	−319.3
3	**3c**	−74.8	−190.2	−142.9	−222.9
4	**3d**	−76.4	−218.2	−172.3	−172.0
5	**3e**	−62.4	−160.4	−140.1	−107.9
6	**3f**	−69.5	−167.8	−233.4	−282.9
7	**3g**	−67.6	−187.7	−90.4	−207.9
8	Chloroquine	−42.4	−157.5	−81.6	−78.7

[a] Emodel score: the minimized poses are rescored using Schrödinger's proprietary GlideScore scoring function and the binding affinity can be estimated by Glide Emodel score, which is the combination of GlideScore (GScore) and nonbonded interaction energy.

[b] eMBrAcE (Multi-Ligand Bimolecular Association with Energetics): ($\Delta E_{Total} = E_{complex} - E_{ligand} - E_{protein}$); *VdW*: van der Waals interaction. ΔE = energy difference (kcal/mol).

2.2. Chemistry

The required α-pyrone C-3 carboxylic acids (**1a**–**b**) were synthesized in two steps from appropriate acetophenones following synthetic methodology reported by our group [15]. Coupling of respective amines with the carboxyl group of **1a**–**b** was carried out using HATU as a coupling reagent [16]. The coupled products (**2a**–**e**) were obtained in more than 70% yield. The methylthio group in **2a**–**d** were replaced with appropriate secondary amines [17] by heating in dioxane to yield **3a**–**d**. Compounds **3e**–**g** were prepared by heating appropriate intermediates (**2a**, **b**, **e**) with H_2O_2 and catalytic amount of acetic acid in dioxane. All the synthesized compounds were characterized by spectral analysis.

2.3. Anti-malarial activity

Antimalarial potentials of **3a-g** were evaluated in an *in-vitro* schizonticidal inhibition assay. All the compounds were found to block life-cycle stage transitions (Table 2) of *Plasmodium falciparum*. The compound **3d** was parasitostatic while others were parasitocidal. The minimum killing concentration (MKC) was the concentration of compounds required to kill parasite present in the culture. Glutathione (GSH), a non-proteinous thiol plays an important role as a cellular redox buffer [18]. The cell health depends on balance between generation and elimination of reactive oxygen/nitrogen species (ROS/RNS), which maintains the redox balance of the cell and proper function of redox-sensitive signaling proteins. Moderate levels of ROS/RNS may function as signals to promote cell proliferation and survival, whereas severe increase of ROS/RNS can induce cell death [19]. GSH is known to directly bind with some ROS species or assist ROS as a source of reductive power for certain antioxidant systems [20]. Therefore, depletion in GSH will imbalance the level of ROS inside cell leading to oxidative stress. Lipids are most susceptible target of oxidative modification through peroxidation that generates lipid radicals, which can further attack the subsequent lipid molecules and propagate as a chain reaction [21]. The lipid peroxides can form adduct with oxidized proteins which in turn can inactivate 26S and 20S proteasomes leading to accumulation of damaged protein and cell death [22]. The lipid peroxidation related cell death is also associated with formation of malondialdehyde (MDA) and 4-hydroxy-2-nonenal (HNE) [23]. In addition, severe damage to the membrane structure might induce membrane perturbation and compromised cellular integrity. As most of our compounds were parasitocidal, we were curious whether they are able to affect the intracellular ROS level. Therefore, to explore such a possibility, we choose **3a**–**d** for study. Compounds **3a**–**c** are parasitocidal with very good MKC and Schinzoticidal Activity while **3d** was parasitostatic (Table 2). The parasite cultures were treated with the sub-lethal concentration of **3a**–**d** individually and change in intracellular ROS, lipid peroxidation (LP) were measured (Table 3). Untreated parasite culture was used to calculate change in oxidative stress indices (ROS and LP) and expressed as fold ± SD. It was found that cells treated with **3a**–**d** had higher ROS level and consequently higher lipid peroxidation

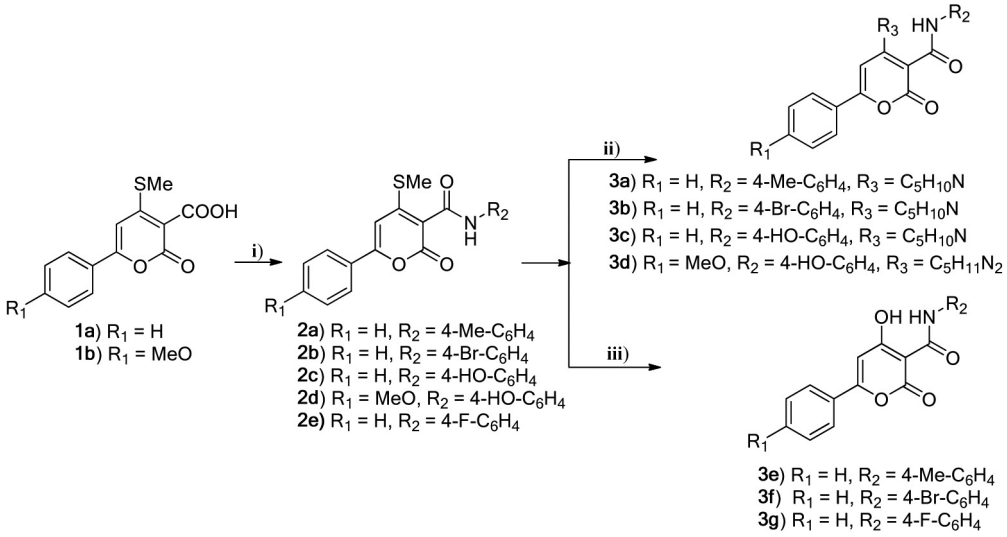

Scheme 1; Reagents and conditions: **i)** R_2NH_2, HATU, DMF, rt, 6h; **ii)** R_3H, Dioxane, 70 °C, 4h; **iii)** H_2O_2, CH_3COOH, Dioxane, 85 °C, 4h.

Scheme 1. Reagents and conditions: i) R_2NH_2, HATU, DMF, rt, 6 h; ii) R_3H, Dioxane, 70 °C, 4 h; iii) H_2O_2, CH_3COOH, dioxane, 85 °C, 4 h.

compared to untreated cells. The results are indicative of several damages to the cellular structure through peroxidation of membrane lipids and may affect proliferation machinery inside the cell. It explains parasiticidal action of most of the α-pyrone derivatives tested in the current study. However, a further detailed study is required to understand the molecular mechanism as well as the cellular machinery involved in the anti-malarial action of these new class of compounds. Also, a PfRIO2 kinase specific assay is needed to understand whether the activity is governed by PfRIO2 kinase.

3. Summary and conclusion

The site identification followed by modeling studies revealed a novel active site within the flexible loop region of PfRIO2 kinase, which can interact with appropriate ligand. The binding mode of designed compounds with target protein was analyzed by IFD molecular docking. Overall, the pharmacophoric hybridization and modeling approach were explored to generate a novel series of α-pyrone molecules for synthesis. All the synthesized molecules showed *in vitro* antimalarial activity. One of the synthesized compounds, **3b**, with most significant result was identified as promising lead for further SAR study. The detailed molecular modeling and chemical modifications are in process to convert this preliminary lead into antimalarial drug candidate.

Table 2
Anti-malarial activities of different α-pyrone analogs (**3a**–**g**).

Comp Code	Schinzoticidal Activity IC_{50} (μM ± SE)	Nature of inhibition	MKC (μM ± SE)
3a	0.859 ± 0.59	Parasitocidal	1.00 ± 0.002
3b	0.337 ± 0.19	Parasitocidal	0.21 ± 0.026
3c	0.765 ± 0.28	Parasitocidal	1.99 ± 0.30
3d	1.568 ± 0.48	Parasitostatic	NA
3e	1.42 ± 0.37	Parasitocidal	38.9 ± 3.82
3f	0.75 ± 0.33	Parasitocidal	3.90 ± 0.59
3g	0.90 ± 0.23	Parasitocidal	2.39 ± 0.33
Chloroquine	0.078 ± 0.012	ND	ND

ND = Not determined.

4. Experimental section/materials and methods

4.1. Computational studies

In absence of PfRIO2 co-crystal structure, our previously described model of PfRIO2 kinase complex with short chain of DNA including ATP was used for current modeling studies [12]. The modeling was carried out using the latest modeling suite from Schrödinger [24]. The Protein Preparation Wizard (PPW) was utilized iteratively to check for any errors related to bond-order, metal charges (+2 for Mn ion), proton assignment, or H-bonding to ensure the chemical correctness of model. The SiteMap program [25,26] can successfully suggest possible binding sites [27]. Therefore, this method was used and "four site points" were disclosed as possible ligand binding site in PfRIO2 kinase (Fig. 2a). The S1 active site was found optimum for ligand binding and used for docking studies. The 3D structure of compounds is treated in LigPrep module of Schrödinger using OPLS2005 force field followed by conformational search analysis through MacroModel [28] using MMFFs force field to obtain the low energy conformer. SiteMap analysis followed by molecular docking [14] of conformationally optimized molecules in S1 active site was used to identify the binding mode of compounds (Fig. 2d). Several docked poses were generated and the best docked poses with lowest Emodel Score were selected for comparative analysis (Table 1). The Emodel energy score has been further verified by the eMBrAcE module of Schrödinger [28]. This module has been used to determine the binding energy differences through minimization using OPLS2005

Table 3
Effect of **3a**–**d** on antioxidant system of malaria parasite.

Compounds	Change in ROS level (fold ± SD[a])	Change in lipid peroxidation (fold ± SD)
Untreated	1	1
3a	1.66 ± 0.14	11.03 ± 0.45
3b	1.87 ± 0.21	4.49 ± 0.26
3c	1.20 ± 0.18	9.03 ± 0.37
3d	1.99 ± 0.20	4.88 ± 0.66

[a] Standard deviation.

force field. The calculations were performed with GB/SA continuum water solvation model. The eMBrAcE minimization was performed for 5000 steps or until the energy difference between subsequent conformations was 0.05 kJ mol^{-1}. The energetic calculations provided energy difference in terms of *VdW*, electrostatic and total ($\Delta E = E_{complex} - E_{ligand} - E_{protein}$). The implicit-water model was used during minimization, conformational search, molecular docking, SiteMap analysis, and energetic calculation.

4.2. Chemistry

4.2.1. General

All reactions were carried out in oven-dried glassware under nitrogen atmosphere. The chemicals and solvents were purchased from Spectrochem, Across, Rankem or Sigma–Aldrich. Melting points were recorded on Veego melting point apparatus. Analytical thin layer chromatography (TLC) was performed on precoated plates (silica gel 60 F-254) purchased from Merck Inc. Purification by gravity column chromatography was carried out on silica gel (100–200 mesh). Electro UV/Vis spectrophotometer was used for recording the UV spectra. $^{1}H/^{13}C$ NMR were obtained from a Varian (400 MHz) spectrometer or Bruker spectrometer using $CDCl_3$ or DMSO-d_6, as solvents. Peaks are recorded with the following abbreviations: s, singlet; bs, broad singlet; d, doublet; t, triplet; q, quartet; m, multiplet; *J*, coupling constant (hertz).

4.2.2. General procedure for the synthesis of **3a–d**

To a solution of an appropriate 2*H*-pyran-4-methylthio-3-carboxamide (**2a–d**, 3.3 mmol) in dioxane, appropriate secondary amine (6.7 mmol) was added and stirred for 4 h at 70 °C. The reaction was monitored by TLC for completion. The solvent was removed under reduced pressure. The ice cold water was added and stirred for 2 h at 0–5 °C. The resulting precipitate was filtered and purified by column chromatography to obtain pure compound.

*4.2.2.1. 2-Oxo-6-phenyl-4-(piperidin-1-yl)-N-(p-tolyl)-2H-pyran-3-carboxamide (**3a**).* Yield: 55%; mp: 133–135 °C; MS-ESI (*m*/*z*): [M^+] 388.6; UV (MeOH) λ_{max} 256.8 nm, 316 nm; IR: (KBr) cm^{-1} 1635, 1674, 2856, 2937, 3275; ^{1}H NMR (400 MHz, DMSO-d_6): δ 1.70 (bs, 6H, $3CH_2$) 2.42 (s, 3H, $ArCH_3$), 3.75 (bs, 4H, $2NCH_2$), 7.50 (s, 1H, CH), 7.55–7.59 (m, 2H, ArH), 8.0–8.05 (m, 5H, ArH), 8.45–8.52 (m, 2H, ArH), 10.82 (s, 1H, NH).

*4.2.2.2. N-(4-Bromophenyl)-2-oxo-6-phenyl-4-(piperidin-1-yl)-2H-pyran-3-carboxamide (**3b**).* Yield: 78%; mp: 210–211 °C; MS-ESI (*m*/*z*): [$M^+ + 2$] 455.0, [M^+] 453.3; UV (MeOH) λ_{max} 259 nm, 324 nm; IR: (KBr) cm^{-1} 1639, 1692, 2843, 2939, 3105, 3325; ^{1}H NMR (400 MHz, $CDCl_3$): δ 1.75 (bs, 6H), 3.56 (bs, 4H), 6.67 (s, 1H), 7.41–7.43 (m, 2H), 7.47–7.50 (m, 3H), 7.57–7.59 (m, 2H), 7.83–7.85 (m, 2H), 10.68 (s, 1H).

*4.2.2.3. N-(4-Hydroxyphenyl)-2-oxo-6-phenyl-4-(piperidin-1-yl)-2H-pyran-3-carboxamide (**3c**).* Yield: 67%; mp: 134–135 °C; MS-ESI (*m*/*z*): [$M^+ + 1$] 391.20; UV (MeOH) λ_{max} 254 nm, 307 nm; IR: (KBr) cm^{-1} 1633, 1666, 2895, 2937, 3184 (broad); ^{1}H NMR (400 MHz, DMSO-d_6): δ 1.75 (bs, 6H, $3CH_2$), 3.55 (bs, 4H, $2NCH_2$), 5.40 (s, 1H, ArOH), 6.65 (s, 1H, CH), 6.79–6.81 (m, 2H, ArH), 7.48–7.50 (m, 5H, ArH), 7.82–7.84 (m, 2H, ArH), 10.36 (s, 1H, NH).

*4.2.2.4. N-(4-Hydroxyphenyl)-6-(4-methoxyphenyl)-4-(4-methylpiperazin-1-yl)-2-oxo-2H-pyran-3-carboxamide (**3d**).* Yield: 31%; mp: >245 °C; MS-ESI (*m*/*z*): [$M^+ + 1$] 436.36; UV (MeOH) λ_{max} 239 nm, 313 nm; IR: (KBr) cm^{-1} 1560, 1612, 1726, 2949, 3066, 3294 (broad); ^{1}H NMR (400 MHz, DMSO-d_6): δ 2.82 (bs, 3H, NCH_3), 3.35–3.42 (m, 8H, $4CH_2$), 4.12 (s, 3H, OCH_3), 7.17–7.19 (d, J = 8 Hz, 1H, ArH), 7.55 (s, 1H, CH), 7.58–7.62 (m, 2H, ArH), 7.76–7.78 (d, J = 8 Hz, 1H, ArH), 7.92–7.94 (d, J = 8 Hz, 1H, ArH), 8.30–8.32 (d, J = 8 Hz, 1H, ArH), 8.50–8.54 (m, 2H, ArH), 9.88 (s, 1H, NH), 11.22 (s, 1H, ArOH).

4.2.3. General procedure for the synthesis of **3e–g**

To a solution 2*H*-pyran-4-methylthio-3-carboxamide (**2a–b**, **e**, 3.3 mmol) in dioxane, 30% (w/w in H_2O) Hydrogen Peroxide solution (6.6 mmol), acetic acid 2–3 drops was added at room temperature. The resulting reaction mixture was stirred at 85 °C for 4 h. The reaction was monitored by TLC for completion. The reaction mixture was diluted with cold water (25 ml) and extracted with DCM, concentrated under reduced pressure. The crude was column purified to get **3e–g**.

*4.2.3.1. 4-Hydroxy-2-oxo-6-phenyl-N-(p-tolyl)-2H-pyran-3-carboxamide (**3e**).* Yield: 35%; mp: 198–199 °C; MS-ESI (*m*/*z*): [$M^+ + 1$] 322.1; UV (MeOH) λ_{max} 247 nm, 340 nm; IR: (KBr) cm^{-1} 1545, 1699, 2906, 3041, 3234; ^{1}H NMR (400 MHz, $CDCl_3$): δ 2.35 (s, 3H, CH_3), 6.65 (s, 1H, CH), 7.17–7.19 (d, J = 8.0 Hz, 2H, ArH), 7.50–7.55 (m, 5H, ArH), 7.87–7.89 (d, J = 6.8 Hz, 2H, ArH), 10.91 (s, 1H, NH).

*4.2.3.2. N-(4-Bromophenyl)-4-hydroxy-2-oxo-6-phenyl-2H-pyran-3-carboxamide (**3f**).* Yield: 40%; mp: 220–222 °C; MS-ESI (*m*/*z*): [M^+] 386.1, [$M^+ + 2$]: 388.2; UV (MeOH) λ_{max} 253 nm, 342 nm; IR: (KBr) cm^{-1} 1597, 1628, 1697, 3101, 3238; ^{1}H NMR (400 MHz, $CDCl_3$): δ 6.67 (s, 1H, CH), 7.48–7.57 (m, 7H, ArH), 7.88–7.90 (d, J = 6.8 Hz, 2H, ArH), 11.02 (s, 1H, NH).

*4.2.3.3. N-(4-Fluorophenyl)-4-hydroxy-2-oxo-6-phenyl-2H-pyran-3-carboxamide (**3g**).* Yield: 30%; mp > 260 °C; MS-ESI (*m*/*z*): [$M^+ - 1$] 323.9; UV (MeOH) λ_{max} 236 nm, 340 nm; IR: (KBr) cm^{-1} 1547, 1637, 1697, 3066, 3236; ^{1}H NMR : (400 MHz, DMSO-d_6): δ 7.02 (s, 1H, CH), 7.14–7.19 (m, 2H, ArH), 7.50–7.55 (m, 3H, ArH), 7.61–7.64 (m, 2H, ArH), 7.86–7.88 (d, J = 6.8 Hz, 2H, ArH), 10.40 (s, 1H, NH).

4.3. Anti-malarial activity

4.3.1. In-vitro schizonticidal inhibition assay

The *in vitro* antimalarial assay was carried out in 96-well microtitre plates as described previously [29,30]. In brief, test compound was incubated with ring stage synchronized *P. falciparum* (3D7) parasitised cell. After 42 h incubation, the blood smears from each well was prepared to record maturation of ring stage parasites into trophozoites and schizonts. MS-Excel Sheet based HN-NonLin program (www.malaria.farch.net) was used to calculate IC_{50} of **3a–g** compounds based on their schizont inhibition profile using regression analysis. To determine the nature of parasite growth inhibition (parasitostatic/parasitocidal), the compounds were removed and the cultures were washed 3 times with albumax II free RPMI-1640 and incubated in complete media with fresh hematocrit for another 72 h. A thin smear was prepared and number of RBCs containing viable parasite was counted. The minimum concentration of compounds giving no viable parasite was used to calculate minimum killing concentration (MKC) of compounds with parasitocidal activity.

4.3.2. Measurements of oxidative stress indices

Parasite cultures were treated with **3a-d** separately. The intracellular ROS was measured by a fluorescent probe (2′,7′-dichlorofluorescein diacetate) and lipid peroxidation was measured as described previously [29,31].

Acknowledgments

This research received funding from Department of Biotechnology (DBT), New Delhi, India through grant no. BT/PR13436/

MED/12/450/2009 & BT/41/NE/TBP/2010. AP is thankful to UGC, India for MANF Junior Research Fellowship. AK and HC acknowledges BIT Mesra for Institute Research Fellowship. AC acknowledges the financial support in the form of a fellowship from IIT-Guwahati. Authors acknowledge Dr. Reddy's Institute of Life Sciences, Hyderabad for NMR-Mass Facility and Central Instrument Facility, BIT Mesra for analytical support.

Appendix A. Supplementary data

Supplementary data related to this article can be found at http://dx.doi.org/10.1016/j.ejmech.2013.10.028.

References

[1] I. Hastings, How artemisinin-containing combination therapies slow the spread of antimalarial drug resistance, Trends Parasitol. 27 (2011) 67–72.
[2] A.P. Phyo, S. Nkhoma, K. Stepniewska, E.A. Ashley, S. Nair, R. McGready, S. Al-Saai, A.M. Dondorp, K.M. Lwin, P. Singhasivanon, Emergence of artemisinin-resistant malaria on the western border of Thailand: a longitudinal study, The Lancet. 379 (2012) 1960–1966.
[3] S. Kumar, U. Bandyopadhyay, Free heme toxicity and its detoxification systems in human, Toxicol. Lett. 157 (2005) 175–188.
[4] V. Trivedi, S. Nag, In silico characterization of atypical kinase PFD0975w from plasmodium kinome: a suitable target for drug discovery, Chem. Biol. Drug Des. 79 (2012) 600–609.
[5] S. Nag, D. Chouhan, S.N. Balaji, A. Chakraborty, K. Lhouvum, C. Bal, A. Sharon, V. Trivedi, Comprehensive screening of heterocyclic compound libraries to identify novel inhibitors for PfRIO-2 kinase through docking and substrate competition studies, Med. Chem. Res. (2013) 1–8.
[6] S. Nag, K. Prasad, V. Trivedi, Identification and screening of antimalarial phytochemical reservoir from northeastern Indian plants to develop PfRIO-2 kinase inhibitor, Eur. Food Res. Technol. 234 (2012) 905–911.
[7] J.B. Koepfli, J.F. Mead, J.A. Brockman, An alkaloid with high antimalarial activity from *Dichroa Febrifuga*1, J. Am. Chem. Soc. 69 (1947), 1837–1837.
[8] S. Jiang, Q. Zeng, M. Gettayacamin, A. Tungtaeng, S. Wannaying, A. Lim, P. Hansukjariya, C.O. Okunji, S. Zhu, D. Fang, Antimalarial activities and therapeutic properties of febrifugine analogs, Antimicrob. Agents Chemother. 49 (2005) 1169–1176.
[9] D. Carmona, J. Saez, H. Granados, E. Perez, S. Blair, A. Angulo, B. Figadere, Antiprotozoal 6-substituted-5,6-dihydro-alpha-pyrones from *Raimondia cf. monoica*, Nat. Prod. Res. 17 (2003) 275–280.
[10] P.L. Chien, C.C. Cheng, Structural modification of febrifugine. Some methylenedioxy analogs, J. Med. Chem. 13 (1970) 867–870.
[11] Y. Zhang, J.A. Clark, M.C. Connelly, F. Zhu, J. Min, W.A. Guiguemde, A. Pradhan, L. Iyer, A. Furimsky, J. Gow, T. Parman, F. El Mazouni, M.A. Phillips, D.E. Kyle, J. Mirsalis, R.K. Guy, Lead optimization of 3-carboxyl-4(1*H*)-quinolones to deliver orally bioavailable antimalarials, J. Med. Chem. 55 (2012) 4205–4219.
[12] D. Chouhan, A. Sharon, C. Bal, Molecular and structural insight into *Plasmodium falciparum* RIO2 kinase, J. Mol. Model. 19 (2013) 485–496.
[13] R.A. Friesner, R.B. Murphy, M.P. Repasky, L.L. Frye, J.R. Greenwood, T.A. Halgren, P.C. Sanschagrin, D.T. Mainz, Extra precision glide: docking and scoring incorporating a model of hydrophobic enclosure for protein–ligand complexes, J. Med. Chem. 49 (2006) 6177–6196.
[14] W. Sherman, T. Day, M.P. Jacobson, R.A. Friesner, R. Farid, Novel procedure for modeling ligand/receptor induced fit effects, J. Med. Chem. 49 (2006) 534–553.
[15] S. Karampuri, P. Bag, S. Yasmin, D.K. Chouhan, C. Bal, D. Mitra, D. Chattopadhyay, A. Sharon, Structure based molecular design, synthesis and biological evaluation of alpha-pyrone analogs as anti-HSV agent, Bioorg. Med. Chem. Lett. 22 (2012) 6261–6266.
[16] L.A. Carpino, 1-Hydroxy-7-azabenzotriazole. An efficient peptide coupling additive, J. Am. Chem. Soc. 115 (1993) 4397–4398.
[17] A. Sharon, P.R. Maulik, C. Vithana, Y. Ohashi, V.J. Ram, Synthesis of biphenanthrenyls and role of C–H···X noncovalent interactions in conformational control, Eur. J. Org. Chem. 2004 (2004) 886–893.
[18] M. Marí, A. Morales, A. Colell, C. García-Ruiz, J.C. Fernández-Checa, Mitochondrial glutathione, a key survival antioxidant, Antioxid. Redox Signal. 11 (2009) 2685–2700.
[19] D. Trachootham, W. Lu, M.A. Ogasawara, N.R.-D. Valle, P. Huang, Redox regulation of cell survival, Antioxid. Redox Signal. 10 (2008) 1343–1374.
[20] V.I. Lushchak, Glutathione homeostasis and functions: potential targets for medical interventions, J. Amino Acids 2012 (2012) 736837.
[21] A.W. Girotti, Lipid hydroperoxide generation, turnover, and effector action in biological systems, J. Lipid Res. 39 (1998) 1529–1542.
[22] D. Poppek, T. Grune, Proteasomal defense of oxidative protein modifications, Antioxid. Redox Signal. 8 (2006) 173–184.
[23] I. Pinchuk, E. Schnitzer, D. Lichtenberg, Kinetic analysis of copper-induced peroxidation of LDL, Biochim. Biophys. Acta 1389 (1998) 155–172.
[24] Schrödinger Suite, LLC, New York, NY, 2012.
[25] SiteMap-V-2.5, V 2.5, Schrödinger, LLC, New York, NY, 2011.
[26] T.A. Halgren, Identifying and characterizing binding sites and assessing druggability, J. Chem. Inf. Model. 49 (2009) 377–389.
[27] M. Nayal, B. Honig, On the nature of cavities on protein surfaces: application to the identification of drug-binding sites, Proteins 63 (2006) 892–906.
[28] MacroModel-V-9.9, Schrödinger, LLC, New York, NY, 2011.
[29] V. Trivedi, P. Chand, K. Srivastava, S.K. Puri, P.R. Maulik, U. Bandyopadhyay, Clotrimazole inhibits hemoperoxidase of *Plasmodium falciparum* and induces oxidative stress. Proposed antimalarial mechanism of clotrimazole, J. Biol. Chem. 280 (2005) 41129–41136.
[30] K.V. Sashidhara, S.R. Avula, G.R. Palnati, S.V. Singh, K. Srivastava, S.K. Puri, J.K. Saxena, Synthesis and in vitro evaluation of new chloroquine–chalcone hybrids against chloroquine-resistant strain of *Plasmodium falciparum*, Bioorg. Med. Chem. Lett. 22 (2012) 5455–5459.
[31] S.N. Balaji, V. Trivedi, Methemoglobin incites primaquine toxicity through single-electron oxidation and modification, J. Basic Clin. Physiol. Pharmacol. 24 (2013) 105–114.